THE JOURNAL OF PHYSICAL CHEMISTRY B LETTERS

**2006,** *110,* 5174−5178
Published on Web 03/01/2006

# Radiative and Nonradiative Rate Fluctuations of Single Colloidal Semiconductor Nanocrystals

**Andreas Biebricher, Markus Sauer,* and Philip Tinnefeld***

*Applied Laser Physics & Laser Spectroscopy, Physics Faculty, University of Bielefeld, Universitätsstr. 25, 33615 Bielefeld, Germany*

*Received: January 31, 2006; In Final Form: February 16, 2006*

Spectrally and time-resolved single-molecule fluorescence spectroscopy was used to investigate fluctuations of the photophysical characteristics of different types of semiconductor nanocrystals (NCs) at room temperature. Correlation of photoluminescence (PL) emission maxima, decay time, and intensity of individual NCs with millisecond time resolution reveals new sources of intensity fluctuations and photophysical properties. In particular, we demonstrate that independent of quenched states spectral diffusion is associated with changes of the radiative rate constant $k_r$ by means of the quantum-confined Stark effect. Correlation of the different photophysical parameters revealed an intrinsic nonradiative rate and enabled the disentangling of intrinsic and extrinsic nonradiative rate constants. Moreover, it allowed us to assess the PL quantum yield of single NCs. Finally, the presented technique was successfully applied to demonstrate that the addition of antiblinking reagents such as mercaptoethylamine accelerates the observed fluctuations between different photophysical states.

Semiconductor nanocrystals, NCs (often denoted as quantum dots), such as core/shell NCs are single crystals a few nanometers in diameter with energy levels directly related to the nanocrystal size. Due to their unique optical properties such as photostability, brightness, and spectral tunability and the possibility of wet chemical synthesis, they have begun impacting a number of disciplines ranging from material science and quantum information processing to biological labeling and imaging applications.[1,2] On the single-particle level, NCs exhibit a number of phenomena such as photon-antibunching,[3] blinking,[4,5] spectral diffusion,[6−8] or the existence of multiple intensity levels correlated with photoluminescence (PL) decay time fluctuations.[9,10] For biological applications, especially if one aims for quantitative analysis of biomolecular interactions on the level of single molecules[11] or for spectral multiplexing, e.g., for ultrahigh-resolution colocalization studies,[12,13] spectral diffusion or "blueing" of the emission as well as changes in the radiative decay time of individual particles can be interfering.[14] Fluctuations in the PL decay time, $\tau$, of individual NCs have so far been attributed to extrinsic variations of the nonradiative rate constant (denoted $k_{nr}^{ext}$), as the decay time always correlated with the intensity caused by trap states that do not completely suppress luminescence.[5,9,10]

Here, we report on additional intensity fluctuations at room temperature which are anticorrelated to the PL decay time, indicating fluctuations of the radiative rate constant $k_r$. Simultaneous measurements of the spectral signature with millisecond temporal resolution demonstrates strong correlation of $k_r$ with spectral diffusion. Furthermore, we find indications for different sources of nonradiative rates, including an intrinsic nonradiative rate not related to external traps, a weakly emissive state, and propose a method for quantum yield measurements of single NCs based on the correlation of different photophysical parameters. The results emphasize that the complex photophysics of NCs can only be resolved with multiparameter approaches on the single-particle level, as otherwise the superposition of the multitude of processes prevents a precise assignment of the observed phenomena.

Details of the confocal microscope system are described in detail elsewhere.[15] For excitation, a 445-nm pulsed diode laser with a repetition rate of 5 MHz (Picoquant GmbH, Berlin) was used. Spectrally resolved and time-resolved PL were recorded with two avalanche photodiodes using appropriate dichroic beam splitters in the detection path.[16,17] To ensure maximum sensitivity, the splitting wavelengths of the beam splitters of 600, 660, and 695 nm were chosen at about the emission maximum $\lambda_{max}$ of the respective NC samples of 605, 655, and 705 nm (Qdot 605, Qdot 655 (both CdSe/ZnS), and Qdot 705 (CdTe/ZnS); Quantum Dot Corporation, Hayward)). Samples were prepared by incubating carefully cleaned cover slides with $10^{-10}$ M solutions of the respective NC sample for 10 s and subsequently drying in nitrogen flow. Measurements were carried out (i) at the glass/air interface, (ii) at the glass/buffer interface, or (iii) covered with immersion oil. The rough spectral signature is represented as fractional intensity $F_2$, i.e., the ratio of the intensity recorded in the long-wavelength channel to the overall luminescence intensity $F_2 = I_{\lambda>\lambda max}/(I_{\lambda<\lambda max} + I_{\lambda>\lambda max})$.[16] The validity of the technique was checked by calibration of the $F_2$ value with the emission wavelength. For this purpose, the emitted light was split by a 50/50 nonpolarizing beam splitter,

* Corresponding authors: M. S. (Phone +49-521-106 5450, Fax +49-521-106-2958, Email sauer@physik.uni-bielefeld.de); P. T. (Phone +49-521-106-5442, Fax +49-521-106-2958, Email tinnefeld@physik.uni-bielefeld.de).

10.1021/jp060660b CCC: $33.50 

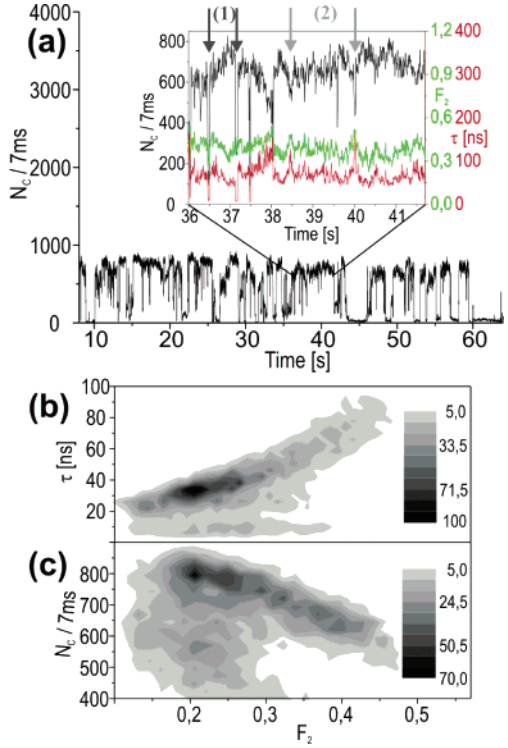


**Figure 1.** (a) PL intensity transient of a single Qdot 655 adsorbed on a glass substrate using an excitation intensity of 0.3 kW/cm$^2$. The inset shows an expanded section of the transient from 36 to 41.7 s (7 ms/bin). The PL intensity, $N_C$ (black) is in most cases anticorrelated to the PL decay time, $\tau$ (red), and $F_2$ value (green). Quenched states indicated by black arrows at 36.5 and 37.2 s (1) are easily recognized by a shortened $\tau$ and decreased $N_C$, whereas for the states with decreased intensity marked by the dark gray arrows at 38.5 and 40.0 s (2), $\tau$ and $F_2$ increase. (b) Density plot of $\tau$ versus $F_2$ and (c) $N_C$ versus PL intensity. Each data point represents one time bin of (a).

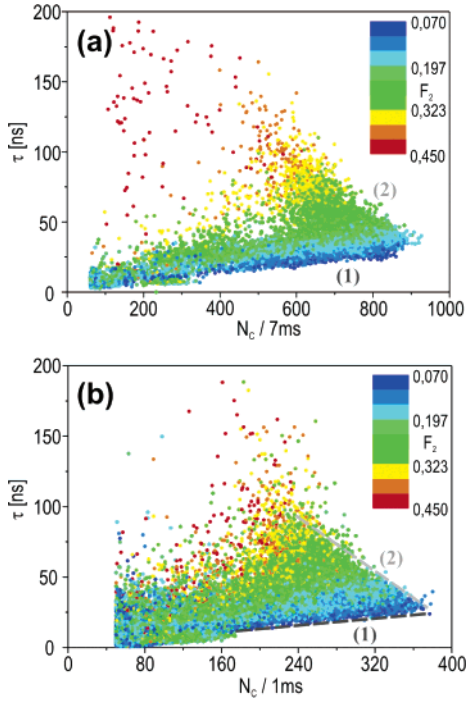


**Figure 2.** (a) Scatter plot of $N_C$ versus $\tau$ for the data shown in Figure 1a (0.3 kW/cm$^2$). (b) Scatter plot for the same NC under saturating conditions, i.e., excitation intensity of 1.4 kW/cm$^2$ and shorter binning time of 1 ms/bin. $F_2$ values are represented by different colors. For clarity, both lower (1) and upper (2) bounds are indicated by a dashed black and dotted gray line, respectively.

and half of the intensity detected by a camera-equipped spectrograph. Emission spectra of 30 individual NCs for each sample were recorded for 1 min simultaneously with the $F_2$ value. For calibration, spectra and $F_2$ values were measured with an integration time (binning) of 1 s. For each bin, the maximum emission wavelength was calculated using a Gaussian fit. The resulting density plots for the $F_2$ wavelength distribution were then fitted using a polynomial function. With the aid of this polynomial function, $F_2$ values could be translated into emission maxima. As the shape of the spectra did not significantly vary during the measurements nor between different NCs, this conversion supplied good spectral information with very high temporal resolution. Time-resolved data were acquired using the FIFO (first-in-first-out) mode of a PC card for time-correlated single-photon counting (SPC 630; Becker & Hickl GmbH, Berlin)[15] from which the PL decay times were derived using a maximum likelihood estimator (MLE) algorithm.[18] The use of a MLE algorithm that yields correct decay times strictly for monoexponential kinetics is justified, because multiexponential deviations of the intrinsically monoexponential NC PL decay are mainly caused by intensity fluctuations due to quenched states.[10] Accordingly, we found that whereas decays integrated over a transient on the minute scale appear multiexponential they are accurately described by a single-exponential model, both for short binning times and for constant intensity levels within the same transient. Influence of multiexciton emission with short decay times was avoided by applying a software delay of 4 ns.[19]

Figure 1a shows a representative luminescence transient of a single Qdot 655 with blinking and different intensity levels beyond mere on−off blinking. The expanded view (inset of Figure 1a) shows the trajectory of the three photophysical parameters, number of counts per bin $N_C$, spectral parameter $F_2$, and PL decay time $\tau$, recorded in a period where the PL emission was close to its maximum intensity, which we denote the "on"-state (e.g., between 36 and 41.7 s with two short interruptions indicated by arrows (1)). Closer inspection reveals a distinct correlation of PL decay time and emission maximum in the "on"-state, i.e., a longer PL decay time is accompanied by a shift of the emission maximum to longer wavelengths. Simultaneously, the PL intensity shows anticorrelated behavior. That is, the PL intensity decreases with increasing decay time and spectral red-shift reflected by the higher $F_2$ value. The correlation is observed in the "on"-state for the complete transient and is further corroborated by the density plots shown in Figure 1b,c in which the $N_C$ and $\tau$ values measured are correlated with the $F_2$ values in time bins of 7 ms. Deviations from the "on"-state population at lower $\tau$ and $N_C$ in the $\tau-F_2$ plot and in the $N_C-F_2$ plot (Figure 1b,c) are caused by quenched states and rapid blinking within the 7-ms bin, respectively. We define quenched states as states with reduced intensity and PL lifetime (see Figure 1a, arrows (1)), whereas blinking is defined as intensity fluctuations between the "on"-state and the background level, i.e., in the case of blinking, $N_C$ is altered, but $\tau$ is not.

Interestingly, the $\tau-N_C$ scatter plots for the same NC shown in Figure 2a feature a wedge-like shape with a clearly defined lower and more diffuse upper bound where $\tau$ increases and decreases, respectively, almost linearly with $N_C$ (labeled (1) and (2), respectively, in Figure 2a). These characteristics were observed for all types of NCs investigated and seem to be a general feature of colloidal NCs, although the relative amplitudes of the subpopulations may vary from dot to dot. Significant influences on the photophysical properties by the nearby dielectric interface[20,21] could be excluded, as the observed

dependencies are not altered after covering the sample with a drop of immersion oil. Both the correlation of the PL decay time with spectral diffusion (Figure 1b) and the anticorrelation with PL emission intensity (Figure 1c) indicate that the $\tau$ fluctuations are not caused by quenched states. Therefore, we strove for extraction of quantitative information out of the experimental data to accurately describe the photophysical characteristics of the observed state with reduced PL intensity but prolonged decay time and red-shifted emission maximum. The PL decay time is determined by the radiative and nonradiative rate constants, $k_r$ and $k_{nr}$, respectively: $\tau = 1/(k_r + k_{nr})$. The number of photons detected per bin, $N_C$, depends on two parameters for a given NC: the absorption cross-section $\sigma$ and the PL quantum yield $\phi$. Otherwise, if we excite the NC under optical saturating conditions with high excitation intensity, the probability for a photon to be absorbed is close to unity, i.e., fluctuations in the absorption cross-section can be neglected. As can be seen in Figure 2b, the scatter plot of $\tau$ versus $N_C$ measured for the same NC under saturating conditions displays the same photophysical characteristics, i.e., the wedge-like shape with a clearly defined upper (indicated by a gray dashed line (2) in Figure 2b) and lower (indicated by a black dotted line (1) in Figure 2b) bound. Hence, the observed shape of the graph is primarily determined by $\phi$ fluctuations, and changes of $\sigma$ can be neglected.

For a constant absorption probability, we can define the PL quantum yield as $\phi = N_C/N_{max}$, where $N_{max}$ is the maximum count rate detected for a given NC which theoretically corresponds to a PL quantum yield $\phi$ of 1.0. Together with the relation $\phi = k_r/(k_r + k_{nr})$, we can distinguish between two possible regimes: PL decay time fluctuations caused by changes of (i) the nonradiative rate constant, $k_{nr}$, or (ii) the radiative rate constant, $k_r$. Assuming that the observed fluctuations in $\tau$ are solely controlled by $k_{nr}$, we obtain eq 1, and accordingly for the case that $\tau$ is a function of $k_r$, we obtain eq 2.

$$\tau(k_{nr}) = (k_r \times N_{max})^{-1} \times N_C \quad (1)$$

$$\tau(k_r) = (k_{nr})^{-1} \times (1 - N_C/N_{max}) \quad (2)$$

The case where $\tau$ is controlled by $k_{nr}$ should be reflected as a linear function through the origin in the $\tau-N_C$ scatter plots, i.e., $\tau$ increases with $N_C$. This region can be associated with the lower bound observed in the $\tau-N_C$ scatter plots (Figure 2b, black line (1)). On the other hand, the upper bound shown in Figure 2b (gray line (2)) can be explained by fluctuations in the radiative rate constant $k_r$. In addition, Figure 2b shows the spectral information (emission maxima) in terms of the $F_2$ value color encoded for each bin. Since the slope of the lower bound depends on $k_r$ (see eq 1), we find different slopes for different colors, i.e., emission maxima. This implies that changes in the emission wavelength of NCs are associated with changes of the radiative rate constant. Further information can be obtained by closer inspection of the slope of the upper bound, which depends inversely proportionally on $k_{nr}$ (eq 2). Here, the negative slope of the upper bound (Figure 2b) implicates a substantial nonradiative rate constant even for maximum PL intensity, i.e., minimum $k_{nr}$. The fact that all investigated NCs exhibit well-defined upper bounds of similar slopes suggests that here $k_{nr}$ is not related to external trap states but rather an intrinsic property of the NCs, which we therefore denote $k_{nr}^{int}$. The overall nonradiative rate can thus be written as $k_{nr} = k_{nr}^{int} + k_{nr}^{ext}$, where $k_{nr}^{ext}$ represents the nonradiative pathways due to external traps.

Furthermore, the linear relationship of the upper bound for high $N_C$ indicates that $k_{nr}^{int}$ is not affected by changes of $k_r$. We

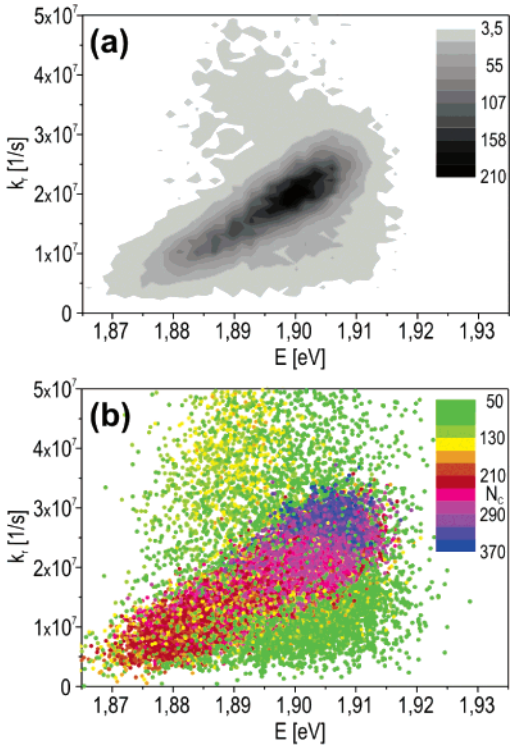


**Figure 3.** (a) Density and (b) scatter plot of the radiative rate constant $k_r$ versus the PL energy $E$ for the data displayed in Figure 2b. The radiative rate was calculated as $k_r = N_C/(\tau \times N_{max})$, whereas $E$ was obtained from the calibrated emission wavelengths. PL intensity $N_C$ is represented by different colors in (b), indicating a weakly emissive state not influenced by the QCSE.

can then extrapolate the linear function to its intersection with the ordinate to obtain $(k_{nr}^{int})^{-1}$, whereas $N_{max}$ can be obtained as the intersection with the abscissa. In the particular case of the NC shown in Figure 2b, we derive $k_{nr}^{int} \approx 1/200$ ns and $N_{max} \approx 430/1$ ms. Hence, we estimate a maximum PL quantum yield of $\phi_{max} = 1 - k_{nr}^{int} \times \tau \approx 0.88$ for the minimum $\tau$ observed in the "on"-state and an average PL quantum yield, $\phi_{av}$ of $\approx 0.75$ excluding quenching by external traps. For the 25 QD 655 investigated, we found intrinsic nonradiative rate constants in the range 1/200−1/300 ns yielding an average $\phi_{av}$ of 0.82 (note that we have chosen a NC with low $\phi_{av}$ in Figures 1 and 2 for better perceptibility of the anticorrelation of $\tau$ and $N_C$). Similar average quantum yields were obtained for the other NC samples, i.e., $\phi_{av} \approx 0.82$ for QD 705 and $\phi_{av} \approx 0.85$ for QD 605. Here, it has to be considered that the calculated PL quantum yields are subject to several uncertainties such as the statistical error of the fitting procedure and the apparent deviations of the upper bound from linear behavior especially for lower PL intensities (indicating a decrease of $k_{nr}^{int}$ with decreasing $\tau$). Nevertheless, our method does not rely on external perturbation[21] and exploits intrinsic fluctuations of photophysical properties. Interestingly, our calculated average quantum yields are located between ensemble values of NCs (that are lower due to dark populations and quenched states) and recent values extracted from similar NC samples in single-molecule experiments.[21,22] As there is no general theory for intrinsic nonradiative rate constants in NCs, available detailed interpretation of the observed dependency would be speculative and requires further investigation.[21,23]

To unravel the origin of the observed decay time fluctuations, the radiative rate constant was calculated as $k_r = N_C/(\tau \times N_{max})$ and plotted versus the PL energy $E$ obtained from the calibrated spectral parameter $F_2$. Figure 3a shows the resulting relatively homogeneous density plot that reveals a clear increase of the

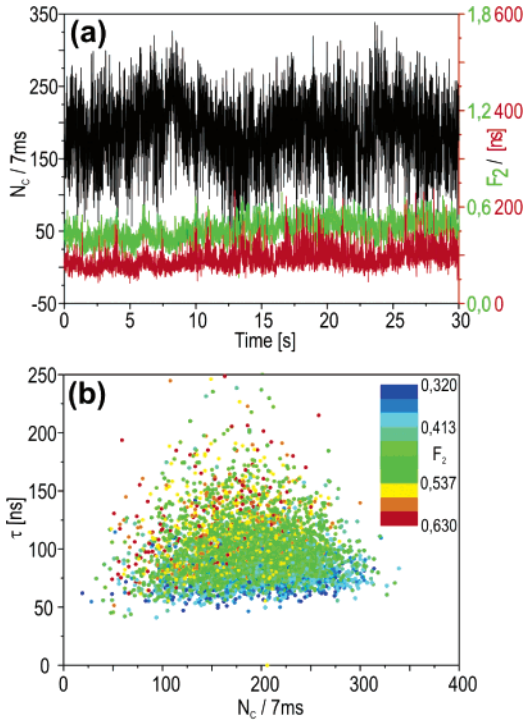


**Figure 4.** (a) PL intensity transient of a single Qdot 705 immobilized in PBS in the presence of 150 mM MEA (0.2 kW/cm$^2$): $N_C$ (black), $\tau$ (red), and $F_2$ value (green) with 7 ms binning. (b) Scatter plot of $N_C$ versus $\tau$ with color-encoded $F_2$ value.

radiative rate constant with increasing PL energy. Since spectral diffusion can be caused by fluctuating charges in the environment of the NC, we assign the observed correlation to the quantum-confined Stark effect (QCSE).[6,24] The QCSE predicts an enlargement of the overlap integral between electron and hole wave functions with increasing energy, thereby increasing the exciton oscillator strength that determines both the radiative rate constant and the absorption cross-section.[25,26] However, the fact that the course of the upper bound is independent of the excitation intensity (compare Figure 2a and b) indicates that the absorption cross-section is only affected at the band edge, whereas excitation occurs at much higher energy (2.8 eV). Albeit no theoretical data about the relationship between energy shift and overlap integral of the electron and whole wave functions exists for the specified NCs, our results are in good qualitative agreement with previous calculations of similar NCs.[27,28] Finally, it has to be pointed out that the correlation of the PL energy with the radiative rate constant is not valid for strongly quenched NC populations (Figure 3b). The strongly quenched states with intensities below 150 counts/ms (green and yellow data points in Figure 3b) are therefore related to a fundamentally different state with broadly scattered radiative rate constants and emission maxima. The fact that this weakly emissive state is not subject to spectral fluctuations caused by the QCSE might be related to emission from a charged NC.

To investigate the role of blinking on the observed photophysical properties, we applied antiblinking agents such as mercaptoethylamine (MEA)[29] on surface-adsorbed NCs in PBS, exemplarily shown for QD 705 in Figure 4a. The scatter plot of the $\tau-N_C$ correlation (Figure 4b) shows a quite homogeneous distribution, and the lower and upper bounds are more difficult to identify. Although the probability of finding a high $F_2$ value is still given at longer PL decay times (Figure 4b), the distribution of the values is much broader in the presence of MEA. Moreover, the lower bound displays a nearly horizontal distribution (compare to Figure 2a,b), which can be attributed to increased blinking kinetics, i.e., significant blinking within a bin of 7 ms which results in decreased $N_C$ without influencing $\tau$. However, the weakened correlation of the photophysical parameters also indicates that spectral diffusion and quenching occur on a faster time scale and are thus subject to averaging effects. These findings implicate an interrelation of spectral diffusion and blinking, which has been inferred from different experiments before.[7] This can be rationalized by the fact that spectral diffusion is caused by charges in the NC environment and blinking indicates loss and recapture of a charge (electron) from the NC into its environment.

In conclusion, new phenomena of individual NCs with different sizes have been revealed by fast and simultaneous spectral and PL decay time measurements applying confocal multiparameter fluorescence microscopy. In particular, fluctuations of the radiative rate constant, $k_r$, induced by the quantum-confined Stark effect and an intrinsic spectrally independent nonradiative rate constant, $k_{nr}^{int}$, were uncovered. Correlation of the different photophysical properties enabled the disentangling of intrinsic and extrinsic nonradiative rate constants and allowed us to assess the PL quantum yield of single NCs. Experiments in the presence of the antiblinking agent MEA emphasize how the observed photophysical properties of NCs might be influenced by the chemical nanoenvironment.

**Acknowledgment.** The authors thank Christian Müller for stimulating discussion. This work was supported by the BMBF (grant 13N8352).

## References and Notes

(1) Alivisatos, A. P. *Science* **1996**, *271*, 933.
(2) Michalet, X.; Pinaud, F. F.; Bentolila, L. A.; Tsay, J. M.; Doose, S.; Li, J. J.; Sundaresan, G.; Wu, A. M.; Gambhir, S. S.; Weiss, S. *Science* **2005**, *307*, 538.
(3) Michler, P.; Imamoglu, A.; Mason, M. D.; Carson, P. J.; Strouse, G. F.; Buratto, S. K. *Nature (London)* **2000**, *406*, 968.
(4) Nirmal, M.; Dabbousi, B. O.; Bawendi, M. G.; Macklin, J. J.; Trautman, J. K.; Harris, T. D.; Brus, L. E. *Nature (London)* **1996**, *383*, 802.
(5) Kuno, M.; Fromm, D. P.; Johnson, S. T.; Gallagher, A.; Nesbitt, D. J. *Phys. Rev. B* **2003**, *67*, 125304/1.
(6) Empedocles, S. A.; Bawendi, M. G. *Science* **1997**, *278*, 2114.
(7) Neuhauser, R. G.; Shimizu, K. T.; Woo, W. K.; Empedocles, S. A.; Bawendi, M. G. *Phys. Rev. Lett.* **2000**, *85*, 3301.
(8) Empedocles, S.; Bawendi, M. *Acc. Chem. Res.* **1999**, *32*, 389.
(9) Schlegel, G.; Bohnenberger, J.; Potapova, I.; Mews, A. *Phys. Rev. Lett.* **2002**, *88*, 137401/1.
(10) Fisher, B. R.; Eisler, H.-J.; Stott, N. E.; Bawendi, M. G. *J. Phys. Chem. B* **2004**, *108*, 143.
(11) Tinnefeld, P.; Sauer, M. *Angew. Chem., Int. Ed.* **2005**, *44*, 2642.
(12) Lacoste, T. D.; Michalet, X.; Pinaud, F.; Chemla, D. S.; Alivisatos, A. P.; Weiss, S. *Proc. Natl. Acad. Sci. U.S.A.* **2000**, *97*, 9461.
(13) Heinlein, T.; Biebricher, A.; Schlueter, P.; Roth, C. m.; Herten, D.-P.; Wolfrum, J.; Heilemann, M.; Mueller, C.; Tinnefeld, P.; Sauer, M. *ChemPhysChem* **2005**, *6*, 949.
(14) Van Sark, W. G. J. H. M.; Frederix, P. L. T. M.; Bol, A. A.; Gerritsen, H. C.; Meijerink, A. *ChemPhysChem* **2002**, *3*, 871.
(15) Weston, K. D.; Dyck, M.; Tinnefeld, P.; Muller, C.; Herten, D. P.; Sauer, M. *Anal. Chem.* **2002**, *74*, 5342.
(16) Tinnefeld, P.; Herten, D. P.; Sauer, M. *J. Phys. Chem. A* **2001**, *105*, 7989.
(17) Ha, T.; Enderle, T.; Chemla, D. S.; Selvin, P. R.; Weiss, S. *Chem. Phys. Lett.* **1997**, *271*, 1.
(18) Tellinghuisen, J.; Wilkerson, C. W., Jr. *Anal. Chem.* **1993**, *65*, 1240.
(19) Fisher, B.; Caruge, J. M.; Zehnder, D.; Bawendi, M. *Phys. Rev. Lett.* **2005**, *94*, 087403/1.
(20) Macklin, J. J.; Trautman, J. K.; Harris, T. D.; Brus, L. E. *Science* **1996**, *272*, 255.
(21) Brokmann, X.; Coolen, L.; Dahan, M.; Hermier, J. P. *Phys. Rev. Lett.* **2004**, *93*, 107403/1.
(22) Ebenstein, Y.; Mokari, T.; Banin, U. *Appl. Phys. Lett.* **2002**, *80*, 4033.

(23) Javier, A.; Magana, D.; Jennings, T.; Strouse, G. F. *Appl. Phys. Lett.* **2003**, *83*, 1423.
(24) Miller, D. A. B.; Chemla, D. S.; Damen, T. C.; Gossard, A. C.; Wiegmann, W.; Wood, T. H.; Burrus, C. A. *Phys. Rev. Lett.* **1984**, *53*, 2173.
(25) Im, J. S.; Kollmer, H.; Off, J.; Sohmer, A.; Scholz, F.; Hangleiter, A. *Phys. Rev. B* **1998**, *57*, R9435.
(26) Larsson, M.; Holtz, P. O.; Elfving, A.; Hansson, G. V.; Ni, W. X. *Phys. Rev. B* **2005**, *71*, 113301/1.
(27) Wen, G. W.; Lin, J. Y.; Jiang, H. X.; Chen, Z. *Phys. Rev. B* **1995**, *52*, 5913.
(28) Menendez-Proupin, E.; Trallero-Giner, C. *Phys. Rev. B* **2004**, *69*, 125336/1.
(29) Hohng, S.; Ha, T. *J. Am. Chem. Soc.* **2004**, *126*, 1324.